


Intestinal Microbiota Dysbiosis Disrupts the Mucosal Barrier, Triggering Inflammatory Responses in Gut-Kidney Interaction and Exacerbating Diarrhea

Junxi Shen^{1,2}, Leyao Fang^{1,2}, Yi Wu^{1,2}, Na Deng^{1,2}, Xinxin Peng^{2,3}, Dandan Li^{1,2}, Zhoujin Tan^{1,2} 

¹School of Traditional Chinese Medicine, Hunan University of Chinese Medicine, Changsha, Hunan, People's Republic of China; ²Hunan Key Laboratory of Traditional Chinese Medicine Prescription and Syndromes Translational Medicine, Changsha, Hunan, People's Republic of China; ³The First Hospital of Hunan University of Chinese Medicine, Changsha, Hunan, People's Republic of China

Correspondence: Zhoujin Tan; Dandan Li, Email tanzhjin@sohu.com; 48797696@qq.com

Purpose: Intestinal microbiota dysbiosis is observed in diarrhea with kidney-yang deficiency syndrome. Therefore, this study will explore the mechanisms by which intestinal microbiota dysbiosis contributes to the initiation and progression of this condition.

Methods: Thirty SPF-grade male KM mice were randomly assigned to three groups: the control group, the diarrhea with kidney-yang deficiency syndrome model group, and the intestinal microbiota dysbiosis + diarrhea with kidney-yang deficiency syndrome model group. After the modeling period, samples were collected. HE staining was employed to observe pathological changes in the colon and kidneys. Detect and analyze the functions of the colonic mucosal barrier and renal function. Measure the levels of NOD-like receptor family pyrin domain containing protein 3 (NLRP3) inflammasome-related molecules and inflammatory factors in the colon and kidney tissues. 16S rRNA sequencing combined with bioinformatics analysis was employed to evaluate the diversity and species composition of the intestinal microbiota, conduct correlation analysis, and predict its metabolic functions.

Results: The model mice exhibited increased fecal water content and decreased body temperature. Structural damage was observed in both the colon and kidney tissues. The intestinal mucosal barrier function was impaired. Furthermore, elevated levels of NLRP3 inflammasome-related molecules and inflammatory cytokines were observed in both colon and kidney tissues. Additionally, alterations were noted in the microbial community structure of the colon contents, characterized by decreased richness, diversity, and evenness. Finally, correlation analysis revealed a significant positive correlation between the characteristic bacterium *Phocaeicola_A* and NLRP3, IL-1 β , and IL-18 in both colon and kidney tissues.

Conclusion: Intestinal microbiota dysbiosis leads to a decline in intestinal mucosal barrier function, accompanied by inflammatory responses and pathological changes in both colonic and renal tissues, resulting in gut-kidney interaction damage. Collectively, these changes promote the development of diarrhea with kidney-yang deficiency syndrome.

Keywords: diarrhea, dysbiosis, gut-kidney interaction, inflammation, intestinal microbiota

Introduction

Diarrhea, defined by loose or watery stools, increased water content, and a higher frequency of defecation, is a condition whose risk factors are linked to food, the environment, and human behavior.¹ As a significant global public health issue, diarrhea resulted in approximately 1.17 million deaths worldwide in 2021.² Traditional Chinese medicine (TCM) categorizes diarrhea into six syndromes based on variations in etiology, pathogenesis, and clinical manifestations. Among these, diarrhea with kidney-yang deficiency syndrome manifests as diarrhea that typically occurs at dawn, with more frequent loose, watery stools, along with cold sensations in the hands and feet and a state of listlessness. Its pathology is complex, and its treatment poses significant challenges. According to TCM, the primary site of this syndrome is the intestine, with the kidney and spleen also being involved.

Concurrently, modern medicine has also established a connection between diarrhea and both the intestine and the kidney. Common contributors to the onset of diarrhea include water loss, electrolyte imbalances, and disruption of colonic epithelial integrity.³ Colonic epithelial cells play a crucial role in regulating luminal secretion, as well as the absorption of fluids and ions, thereby modulating the transport of fluids and electrolytes and maintaining intestinal and systemic homeostasis.⁴ Diarrhea-induced dehydration is a primary prerenal factor contributing to acute kidney injury, resulting in a rapid decline in renal filtration function and a sustained increase in serum creatinine levels.⁵ Kidney transplant recipients frequently experience diarrhea post-transplant, characterized by reduced bacterial diversity and commensal richness in their stool samples. Most early post-transplant diarrhea cases are primarily associated with dysbiosis, rather than common infectious diarrheal pathogens.⁶ Hence, there is a close pathophysiological relationship between diarrhea and intestinal and renal functions. When exploring the specific pathological mechanisms of diarrhea associated with kidney-yang deficiency syndrome, it is imperative to consider the intestinal and renal functions holistically, along with their interactions.

Drawing on both TCM theories and the modern medical concept of the gut-kidney axis, our team successfully established a mouse model of diarrhea with kidney-yang deficiency syndrome by administering adenine combined with *Folium sennae* decoction via gavage. We observed increased microbial activity in the intestinal contents and decreased activity in the intestinal mucosa of the model mice. Renal function was impaired, and a correlation was found between renal function and both intestinal enzyme activity and microbial activity.^{7,8} Microbial activity serves as a crucial indicator reflecting the metabolic capacity of microorganisms. In the context of this disease state, the disparities in microbial activity across different segments of the intestine are likely linked to the structural and functional differences inherent in these regions.

In mice with diarrhea with kidney-yang deficiency syndrome, there was a decrease in the counts of *Lactobacillus* and *Bifidobacterium* in the small intestinal contents, along with an increase in the total bacterial count and the number of *Escherichia coli*. Renal interstitial dilatation, inflammatory cell infiltration, and elevated levels of malondialdehyde (MDA) and superoxide dismutase (SOD) in the kidneys suggested increased oxidative stress.⁹ Decreased expression of occludin and zonula occludens-1 (ZO-1) proteins in the small intestine indicated disruption of the intestinal mucosal barrier, and serum levels of NOD-like receptor family pyrin domain containing protein 3 (NLRP3), Interleukin (IL)-1 β , and transforming growth factor (TGF)- β 1 were significantly elevated.¹⁰ Dysbiosis of the cecal microbiota, characterized by a reduction in beneficial bacteria, potentially increased choline trimethylamine lyase activity, leading to elevated levels of the inflammatory cytokines IL-6 and tumor necrosis factor (TNF)- α .¹¹ These findings suggest that mice with diarrhea with kidney-yang deficiency syndrome exhibit intestinal microbiota dysbiosis, impaired intestinal and renal functions, and heightened levels of inflammation and oxidative stress.

The intestinal microbiota plays a crucial role in maintaining host health. It is currently known that the intestinal microbiota is a key participant in the bidirectional interaction of the gut-kidney axis, exerting vital effects on the physiological functions of both the host's kidneys and intestines.¹² Dysbiosis of the intestinal microbiota, increased intestinal permeability, and damage to the intestinal barrier can occur together. These conditions allow luminal intestinal antigens, pro-inflammatory factors, and metabolites to enter intestinal tissues. This creates a vicious cycle of tight junction damage and inflammation. Consequently, it exacerbates the persistent systemic inflammatory state in patients with chronic kidney disease (CKD).¹³ NLR-like receptors in the intestinal epithelium, serving as pathogen sensors, recognize PAMPs, activate downstream signaling pathways, and induce immune molecule expression, thereby promoting mucosal immune responses.¹⁴ When the host's intestinal microbiota is disrupted, pathogenic bacteria overgrow. This overgrowth is positively correlated with an increase in pathogenic bacteria in the peripheral blood. Meanwhile, the circulatory system accumulates more metabolites, such as lipopolysaccharide (LPS), urea, phosphorus. These changes accelerate disease progression.¹⁵ The addition of probiotics (such as *Lactobacillus rhamnosus*) can slow down the decline in renal function and inflammatory state in CKD mice, significantly reducing the concentration levels of serum creatinine, blood urea nitrogen, and serum IL-6.¹⁶ Intestinal microbiota, acting as a critical mediator between the intestinal and kidney, maintains functional integrity of the bidirectional gut-kidney axis under physiological conditions.

Given the significant role of the intestinal microbiota in the gut-kidney axis as discussed above, we hypothesize that the interaction between the intestine and the kidney, mediated by the intestinal microbiota, is linked to the development

of diarrhea with kidney-yang deficiency syndrome. This study will further delve into the specific disease mechanisms underlying diarrhea with kidney-yang deficiency syndrome, with a focus on the gut-kidney interaction mediated by intestinal microbiota dysbiosis.

Materials and Methods

Preparation of Experimental Animals

This research has been approved by the Institutional Animal Care and Use Committee of Hunan University of Chinese Medicine (ethics approval number: HNUCM21-2409-14), and all experimental programs and operations were conducted in strict compliance with the Laboratory Animal—Guideline for Ethical Review of Animal Welfare (GB/T 35892–2018). Thirty SPF-grade KM mice, weighing 18–22g and of male sex,¹⁷ were used in this study. This experiment employed mice of a single sex. The mice were purchased from Hunan Slaccas Jingda Laboratory Animal Co., Ltd. (Animal License No. SCXK(Hunan)2019-0004) and housed at the Experimental Animal Center of Hunan University of Chinese Medicine. The environmental conditions for the experimental animals were maintained at a room temperature of 23–25 °C, a relative humidity of 50%–70%, with a 12-hour light/dark cycle, and the animals had free access to food and water.

Information on Animal Feed

During the experiment, SPF-grade maintenance feed for mice and rats was used, which was uniformly provided by the Experimental Animal Center of Hunan University of Chinese Medicine. The feed was manufactured by Beijing HFK Bioscience Co., Ltd., with a Feed Production License number of Beijing Feed Production License (2019)06076 and a production batch number of 410250416.

Reagents and Reagent Kits

The enzyme-linked immunosorbent assay (ELISA) kits for IL-1 β (Cat. No.: M-02323M1, Lot NO.: 202,405), IL-18 (Cat. No.: JM-02452M1, Lot NO.: 202,405), TNF- α (Cat. No.: JM-02415M1, Lot NO.: 202,405), diamine oxidase (DAO, Cat. No.: JM-02511M1, Lot NO.: 202,405), NLRP3 (Cat. No.: JM-02936M1, Lot NO.: 202,405), caspase-1 (Cat. No.: JM-02511M1, Lot NO.: 202,405), and caspase-1-p20 (Cat. No.: JM-11880M1, Lot NO.: 202405) were all manufactured by Jiangsu Jingmei Biotechnology Co., Ltd. Adenine was sourced from Biofroxx (Germany) with Cat. No.: 1163GR005 and Lot NO.: EZ7890B179. Gentamicin Sulfate Injection was manufactured by Yichang Humanwell Pharmaceutical Co., Ltd. with production batch number 3C3111912. Cefradine Capsules were produced by Shandong Lukang Pharmaceutical Co., Ltd. with production batch number 53240212. *Folium sennae* were manufactured by Bozhou Huqiao Pharmaceutical Co., Ltd. with production batch number 2311300022.

Drug Preparation

Preparation of adenine suspension:¹⁸ Adenine was prepared at a dosage concentration of 5 mg·mL⁻¹ using sterile distilled water. The suspension was prepared fresh for immediate use.

Preparation of *Folium sennae* decoction:¹⁹ *Folium sennae* was placed in a beaker and soaked in water at a weight ratio of 1:5 for 30 min. The mixture was then heated in a water bath at 75 °C for 30 min, followed by filtration to collect the filtrate. The residue was then mixed with an appropriate amount of water, heated again in a water bath at 75 °C for 15 min, and filtered to collect the second filtrate. The two filtrates were combined and concentrated at 75 °C to obtain a *Folium Sennae* decoction with a concentration of 1 g·mL⁻¹ of crude drug. The decoction was stored at 4 °C for future use.

Preparation of mixed antibiotic solution:^{20,21} A mixed antibiotic solution with a concentration of 62.5 g·L⁻¹ was prepared using gentamicin injection and cefradine capsules.

Animal Grouping and Intervention

After a 3-day period of adaptive feeding, 30 mice were randomly assigned to three groups: the control group (CC), the diarrhea with kidney-yang deficiency syndrome group (CM), and the intestinal microbiota dysbiosis + diarrhea with kidney-yang deficiency syndrome group (CMM), with 10 mice in each group. The models for intestinal microbiota dysbiosis^{22,23} and

diarrhea with kidney-yang deficiency syndrome were established according to previous methods developed by our research team,¹⁰ over a total duration of 14 days. From days 1 to 14, both CM and CMM groups were administered adenine suspension ($50 \text{ mg} \cdot \text{kg}^{-1}$) via gavage once daily. During days 1–7, mice in the CMM group were administered a mixed antibiotic solution ($23.33 \text{ mL} \cdot \text{kg}^{-1} \cdot \text{d}^{-1}$) via gavage twice daily. During days 8–14, both CM and CMM groups were also administered *Folium sennae* decoction ($10 \text{ g} \cdot \text{kg}^{-1}$) via gavage once daily. Mice in the CC group were administered sterile water (0.35 mL) via gavage twice daily for 14 consecutive days.

Observation of General Conditions in Animals

The mental status, spontaneous activity, fecal morphology and color, as well as the cleanliness around the anus of mice in each group were observed. On the 14th day of model establishment, fecal samples were collected from the mice, and rectal temperatures were measured. Fecal water content was determined by weighing the wet weight of the fecal samples, drying the samples to a constant weight at 110°C , recording the dry weight, and then calculating the fecal water content using the formula: Fecal Water Content = (Wet Fecal Weight - Dry Fecal Weight) / Wet Fecal Weight $\times 100\%$.²⁴

Sample Collection

After the completion of the modeling cycle, the mice were anesthetized, and blood samples were collected from the mice. The mice were then euthanized by cervical dislocation, and their kidneys were collected for further analysis. Under sterile conditions, colonic contents were collected using sterile forceps. Subsequently, the colon was cut open longitudinally using surgical scissors, rinsed clean with physiological saline, and then stored.^{25,26}

Histopathological Examination of Kidney and Intestine Samples

Colon and kidney tissues fixed in 4% paraformaldehyde were dehydrated with graded ethanol, embedded in paraffin, sectioned, and then stained with Hematoxylin and Eosin (HE). After gradient dehydration, the sections were mounted with neutral resin and observed under a light microscope for pathological changes in the colon and kidney tissues.

Immunohistochemical Detection of ZO-1 and Occludin Proteins in the Colon

Paraffin-embedded colon sections were subjected to antigen retrieval and serum blocking, followed by incubation with primary antibodies against ZO-1 and occludin at 4°C overnight. After washing with PBS and drying, the sections were covered with HRP-labeled secondary antibodies and incubated at room temperature for 1 hour. Color development was performed using 3,3'-Diaminobenzidine (DAB) substrate, with the reaction time controlled under a microscope. The sections were then counterstained with hematoxylin for 3 minutes, dehydrated, mounted, and examined under a microscope. The average optical density (AOD) of the sections was measured using Image software.

Biochemical Assay of Serum BUN and Cr

Whole blood samples were allowed to stand for 4 hours, then centrifuged at 3000 revolutions per minute (rpm) for 10 min at 4°C . The upper layer of serum was collected, and the concentrations of blood urea nitrogen (BUN) and creatinine (Cr) in the serum were measured using an automated biochemical analyzer.

ELISA-Based Detection of Serum DAO and Measurement of NLRP3

Inflammasome-Related Molecules and Inflammatory Cytokines in Colon and Kidney Tissues

Serum samples were collected to measure the concentration of DAO. Colon and kidney samples were obtained and homogenized using a tissue grinder. The homogenates were then centrifuged at 3000 rpm for 10 min at 4°C . The supernatants were collected to determine the levels of IL-1 β , IL-18, TNF- α , NLRP3, caspase-1, and caspase-1-p20 in the colon and kidney.²⁷ Sample addition, enzyme addition, incubation, plate washing, color development, and reaction termination were performed according to the kit instructions. The optical density (OD) values were measured using a microplate reader, and standard curves were plotted to calculate the concentration of each cytokine in the samples.

High-Throughput Sequencing of 16S rRNA Genes From Colon Contents

The colon content samples underwent grinding pretreatment, and nucleic acids were extracted from the samples using the OMEGA Soil DNA Kit (D5635-02) (Omega Bio-Tek, Norcross, GA, USA). DNA quantification was carried out with a Nanodrop NC2000 (Thermo Scientific, USA), and the quality of the extracted DNA was evaluated through agarose gel electrophoresis. Standard bacterial 16S rRNA V3-V4 region primers, with the forward primer sequence 338F (5'-ACTCCTACGGGAGGCAGCA-3') and the reverse primer sequence 806R (5'-GGACTACHVGGGTWTCTAAT-3'), were selected for PCR amplification. The PCR amplified and recovered products were fluorescently quantified using the Quant-iT PicoGreen dsDNA Assay Kit on a Microplate reader (BioTek, FLx800). Sequencing libraries were constructed using the TruSeq Nano DNA LT Library Prep Kit (Illumina). Qualified libraries were subjected to paired-end sequencing of 2×250 bp on an Illumina NovaSeq machine using the NovaSeq 6000 SP Reagent Kit (500 cycles). Sequencing was performed by Shanghai Personal Biotechnology Co., LTD (Shanghai, China).

Bioinformatics Analysis

1. Sequence Processing and Species Annotation: Raw sequencing data were denoised using the QIIME2 DADA2 pipeline to obtain amplicon sequence variants (ASVs). The feature sequences of ASVs were then aligned against reference sequences in the Greengenes database for taxonomic annotation of species. For each sample in the ASV abundance matrix, random sampling of the total sequences was performed at different depths. Using the sequence counts and corresponding ASVs sampled at each depth, the data were normalized, and rarefaction curves were generated based on the ASV abundance data.
2. Alpha Diversity Analysis: Alpha diversity indices, including the Chao1 index, Pielou's evenness index, Shannon index, and Simpson index, were calculated for samples in each group to compare changes in intestinal microbiota structure, richness, diversity, and evenness among the groups.
3. Beta Diversity Analysis: The Bray-Curtis distance algorithm was used to analyze changes in microbial community structure between samples. Visualization was achieved through principal coordinates analysis (PCoA) and non-metric multidimensional scaling (NMDS) methods.
4. Characteristic Microbiota Analysis: linear discriminant analysis effect size (LEfSe) analysis was employed, utilizing an all-against-all (more strict) comparison strategy with an LDA threshold set to less than 2, to perform differential analysis across all taxonomic levels for samples between groups. Using the non-rarefied ASV/OTU table, the "classify_samples_ncv" function in q2-sample-classifier was invoked for Random Forest analysis.
5. Correlation Analysis: Spearman correlation coefficient was utilized to analyze the correlation between characteristic bacteria in colonic contents and NLRP3, IL-1 β , and IL-18 in the colon and kidney.
6. Metabolic Pathway Prediction: The composition of intestinal microbiota metabolic pathways was inferred using PICRUST2 with information from the MetaCyc database.

Statistical Analysis

Statistical analysis and graphing were performed using GraphPad Prism 8.0 software. Data for each group are presented as the mean \pm standard deviation (mean \pm SD). For data following a normal distribution, one-way ANOVA was used for comparisons between multiple groups, with Tukey's method applied for intergroup comparisons. For data not following a normal distribution, the Mann-Whitney *U*-test was used. A $p < 0.05$ was considered statistically significant, and a $p < 0.01$ was considered highly statistically significant.

Results

General Characteristics of Mice in Each Group

Mice in the CC group exhibited normal mental status and spontaneous activity. Their bedding was dry, and their feces were well-formed with moderate consistency, not easily adhering to the bedding. Their anal areas were clean. In contrast, mice in the CM and CMM groups showed poor mental status, reduced spontaneous activity, and a tendency to huddle together. Their bedding was damp, and their feces were loose, unformed, and prone to adhering to the bedding, with fecal

material attached to the anal area, indicating poor cleanliness. Feces of mice in the CMM group were lighter in color. Compared to the CC group, the fecal water content was significantly increased in the CM and CMM groups ($p < 0.01$). Additionally, rectal temperatures were significantly decreased in the CM ($p < 0.05$) and CMM ($p < 0.01$) groups compared to the CC group. These findings suggest that the modeling process altered the general characteristics of the mice (Figure 1).

Morphological Changes in Colon and Kidney Tissues of Mice in Various Groups

As shown in Figure 2A, HE staining of the colon revealed that the colonic tissue structure in the CC group exhibited no significant abnormalities. The crypts were arranged in a parallel and orderly manner, and there was no obvious abnormal inflammatory infiltration (as indicated by the white arrows in Figure 2A). In the CM group, there was atrophy and branching of the crypt tissue (as indicated by the yellow arrows in Figure 2A), along with an increased number of inflammatory cells and abnormal inflammatory infiltration (as indicated by the red arrows in Figure 2A). In the CMM group, there was atrophy and branching of the crypt tissue (as indicated by the yellow arrows in Figure 2A). A large number of inflammatory cells and abnormal inflammatory infiltration were observed in the field of view (as indicated by the red arrows in Figure 2A), accompanied by lymphocyte aggregation at the base (as indicated by the blue arrow in Figure 2A).

As shown in Figure 2B, HE staining of the kidneys revealed that in the CC group, the renal cortex exhibited a clear structure, with no significant change in glomerular volume. The Bowman's capsule space was clearly visible, and the renal tubules showed no atrophy or dilation (as indicated by the white arrows in Figure 2B). Moreover, no significant inflammatory cell infiltration was noted in the interstitium. In the CM group, the renal cortex structure was damaged. Numerous inflammatory cells were observed within the glomeruli, and the Bowman's capsule space appeared unclear (as indicated by the yellow arrows in Figure 2B). Additionally, the volume of renal tubular epithelial cells was increased (as indicated by the red arrows in Figure 2B). In the CMM group, the renal cortex structure was also damaged. There was an increase in glomerular volume, and numerous inflammatory cells were visible within the glomeruli. The Bowman's capsule space was unclear (as indicated by the yellow arrows in Figure 2B). The renal tubules exhibited irregular luminal structure and congestion (as indicated by the red arrows in Figure 2B), and inflammatory cell infiltration was present in the interstitium (as indicated by the blue arrows in Figure 2B).

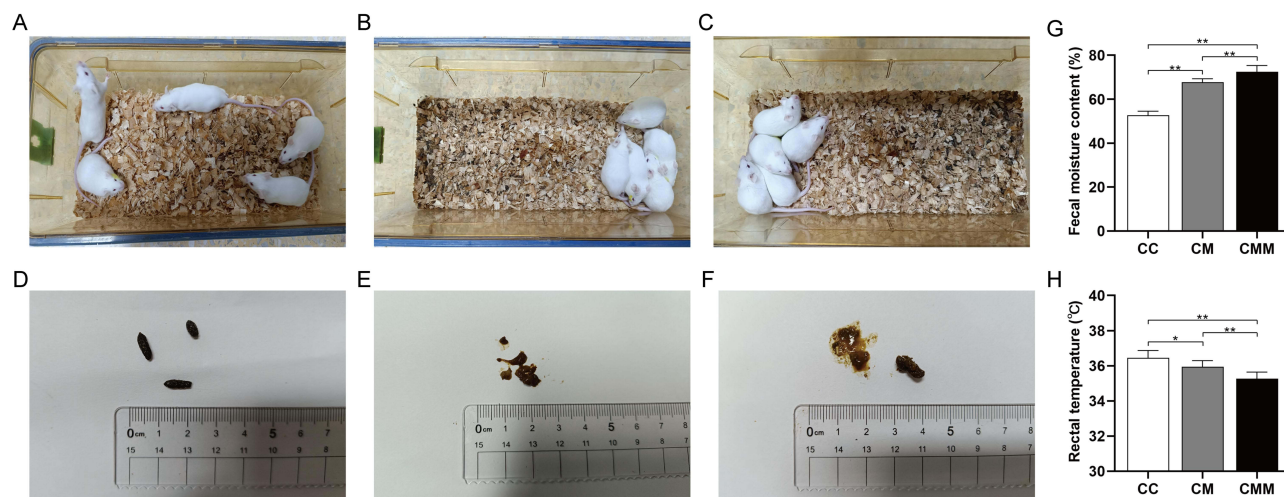


Figure 1 General conditions of mice in each group. (A) Mental status and bedding condition of mice in the CC group; (B) Mental status and bedding condition of mice in the CM group; (C) Mental status and bedding condition of mice in the CMM group; (D) Feces of mice in the CC group; (E) Feces of mice in the CM group; (F) Feces of mice in the CMM group; (G) Fecal water content in mice from each group ($n=6$); (H) Rectal temperature of mice in each group ($n=10$). * $p < 0.05$; ** $p < 0.01$.

Abbreviations: CC, control group; CM, diarrhea with kidney-yang deficiency syndrome group; CMM, intestinal microbiota dysbiosis + diarrhea with kidney-yang deficiency syndrome group.

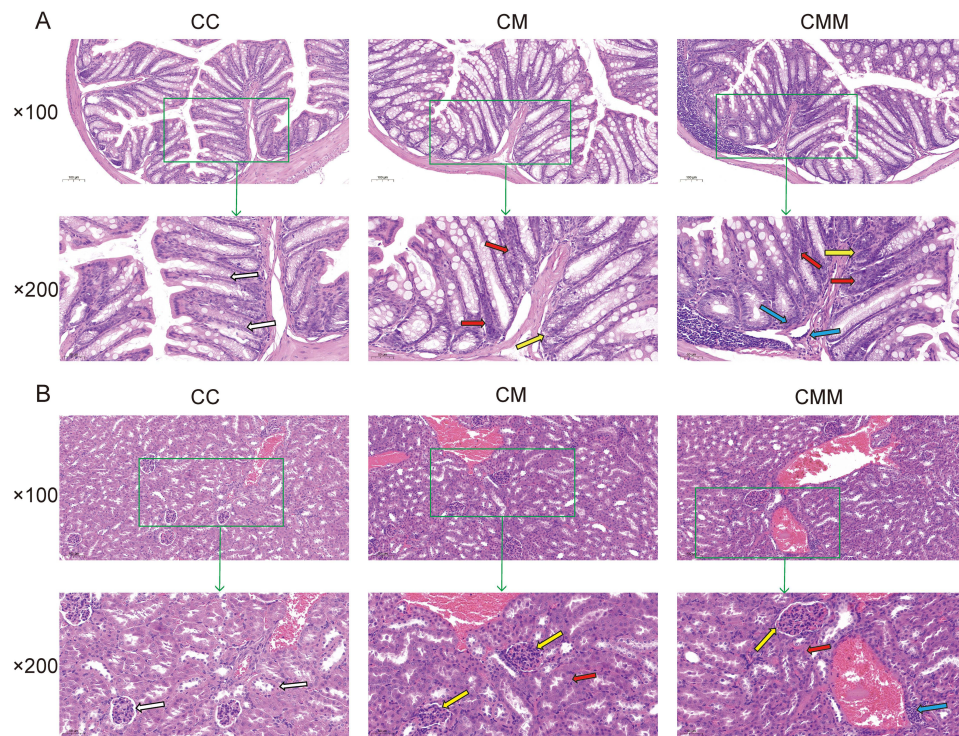


Figure 2 Observation of colonic and kidney tissue changes in mice using HE staining. **(A)** HE staining of colonic tissue in various groups ($\times 100$, $\times 200$); **(B)** HE staining of kidney tissue in various groups ($\times 100$, $\times 200$). In **Figure 2A**, white arrows indicate normal crypt structure; yellow arrows indicate abnormal crypt structure; red arrows indicate inflammatory cell infiltration; and blue arrows indicate lymphocyte aggregation. In **Figure 2B**, white arrows indicate normal renal tissue structure; yellow arrows indicate abnormal renal corpuscle structure; red arrows indicate abnormal renal tubular structure; and blue arrows indicate interstitial inflammatory cell infiltration.

Abbreviations: CC, control group; CM, diarrhea with kidney-yang deficiency syndrome group; CMM, intestinal microbiota dysbiosis + diarrhea with kidney-yang deficiency syndrome group.

Changes in Indicators Related to Colonic Mucosal Barrier Function in Mice From Various Groups

Compared with the CC group, the expression of occludin protein in the colonic tissue of the CM group decreased, but there was no significant difference ($p > 0.05$); the expression of occludin protein in the colonic tissue of the CMM group was significantly decreased ($p < 0.05$). The expression of ZO-1 protein in the colonic tissue of both the CM and CMM groups was significantly decreased ($p < 0.01$). Compared with the CC group, significant rises in the serum levels of DAO were observed in the CM and CMM groups (CM group: $p < 0.05$, CMM group: $p < 0.01$) (**Figure 3**). These results suggest the presence of intestinal mucosal barrier dysfunction in the setting of diarrhea with kidney-yang deficiency syndrome.

Changes in Renal Function in Mice From Various Groups

Compared to the CC group, serum BUN levels were significantly increased in both the CM and CMM groups ($p < 0.01$), and serum Cr levels were also significantly elevated (CM group: $p < 0.05$; CMM group: $p < 0.01$), indicating renal function impairment in mice with diarrhea with kidney-yang deficiency syndrome (**Figure 4**).

Levels of NLRP3 Inflammasome-Related Molecules and Inflammatory Factors in Colon Tissue

Compared with the CC group, the levels of NLRP3 and IL-18 in the colonic tissues of mice in the CM and CMM groups were markedly elevated ($p < 0.05$ for the CM group, $p < 0.01$ for the CMM group). The levels of Caspase1-p20 in the colonic tissues of the CM and CMM groups were significantly elevated ($p < 0.05$ for the CM group, $p < 0.01$ for the CMM group). Additionally, the Caspase-1 levels in the colonic tissues of the CM and CMM groups were significantly increased ($p < 0.01$). The IL-1 β levels in the colonic tissues of the CM and CMM groups were also significantly elevated ($p < 0.05$ for the CM group, $p < 0.01$ for the

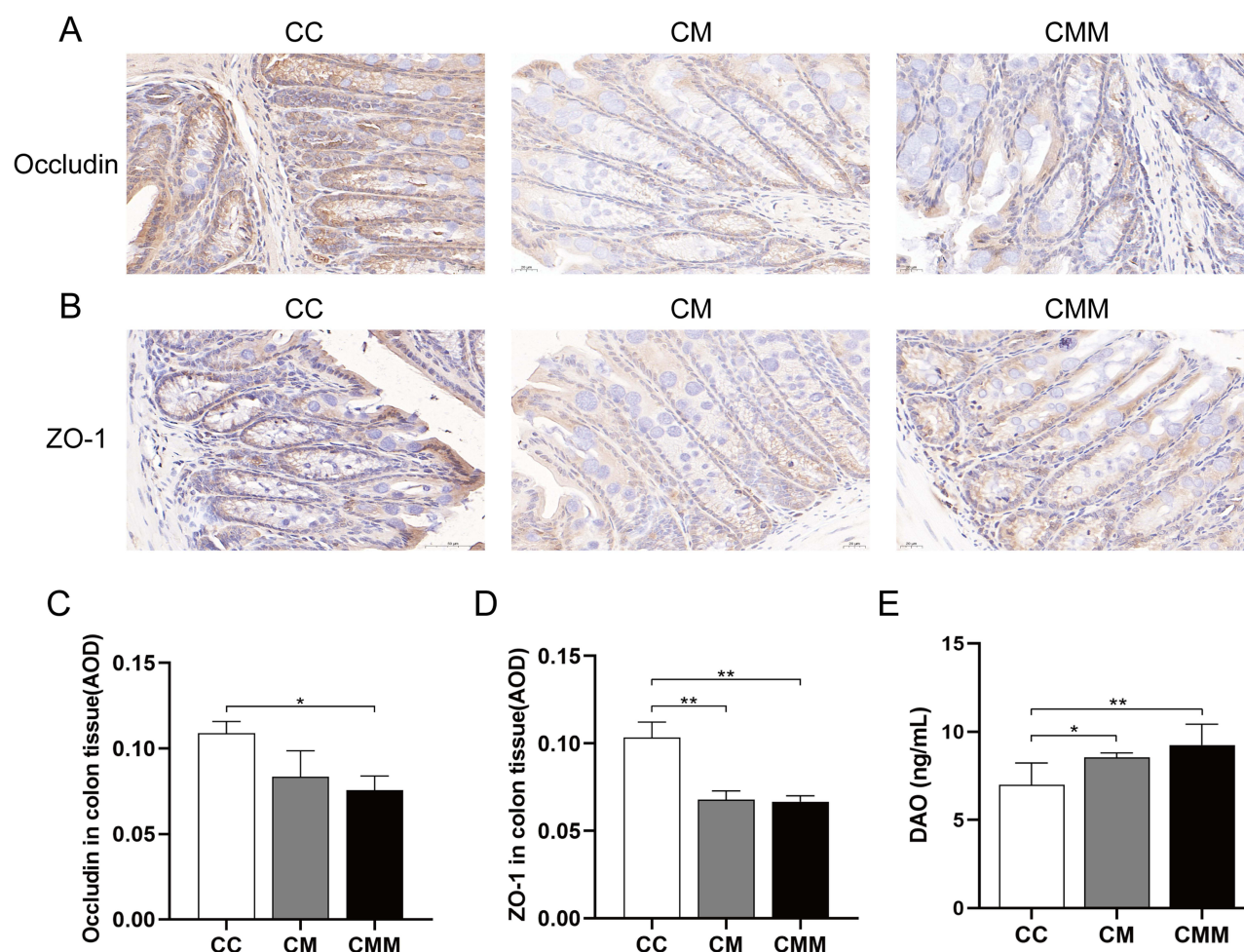


Figure 3 Status of molecules related to intestinal mucosal barrier function in mice from various groups. **(A)** Expression of occludin protein in colonic tissue (IHC, ×400); **(B)** Expression of ZO-1 protein in colonic tissue (IHC, ×400); **(C)** AOD of occludin protein in colonic tissue (n=3); **(D)** AOD of ZO-1 protein in colonic tissue (n=3); **(E)** Serum levels of DAO (n=6). * $p < 0.05$; ** $p < 0.01$.

Abbreviations: CC, control group; CM, diarrhea with kidney-yang deficiency syndrome group; CMM, intestinal microbiota dysbiosis + diarrhea with kidney-yang deficiency syndrome group.

CMM group). The TNF- α levels in the colonic tissues of mice in the CMM group were distinctly higher ($p < 0.05$), while those in the CM group were increased but did not reach statistical significance. Compared with the CM group, the CMM group had significantly higher levels of Caspase1-p20 in the colonic tissues with a statistically significant difference ($p < 0.05$), and the IL-1 β levels in the colonic tissues of the CMM group were also significantly higher ($p < 0.01$). Indicating elevated levels of NLRP3, Caspase-1, Caspase1-p20, IL-1 β , IL-18, and TNF- α in the colonic tissues of mice with kidney-yang deficiency syndrome accompanied by diarrhea (Figure 5).

Levels of NLRP3 Inflammasome-Related Molecules and Inflammatory Factors in Kidney Tissue

Compared with the CC group, the levels of NLRP3 and IL-18 in kidney tissues were significantly increased in the CM and CMM groups ($p < 0.01$). In the CMM group, the levels of Caspase1-p20 and Caspase-1 in kidney tissues were also markedly upregulated ($p < 0.01$). The levels of IL-1 β in kidney tissues were significantly higher in both the CM and CMM groups ($p < 0.05$ for the CM group, $p < 0.01$ for the CMM group). The levels of TNF- α in kidney tissues were significantly increased in the CM group ($p < 0.05$) and even more so in the CMM group ($p < 0.01$). Compared with the CM group, the levels of Caspase1-p20 and Caspase-1 were significantly higher in kidney tissues of the CMM group ($p < 0.05$). Additionally, IL-18 levels were also significantly elevated in kidney tissues of the CMM group ($p < 0.01$). Increased levels of NLRP3, Caspase-1, Caspase1-

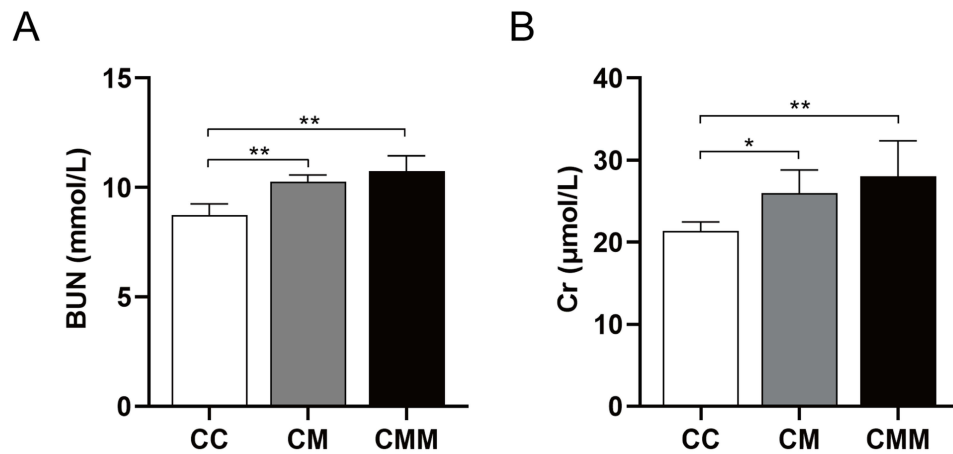


Figure 4 Renal function status in mice from various groups. (A) Serum BUN levels; (B) Serum Cr levels (n=6). * $p < 0.05$; ** $p < 0.01$.

Abbreviations: CC, control group; CM, diarrhea with kidney-yang deficiency syndrome group; CMM, intestinal microbiota dysbiosis + diarrhea with kidney-yang deficiency syndrome group.

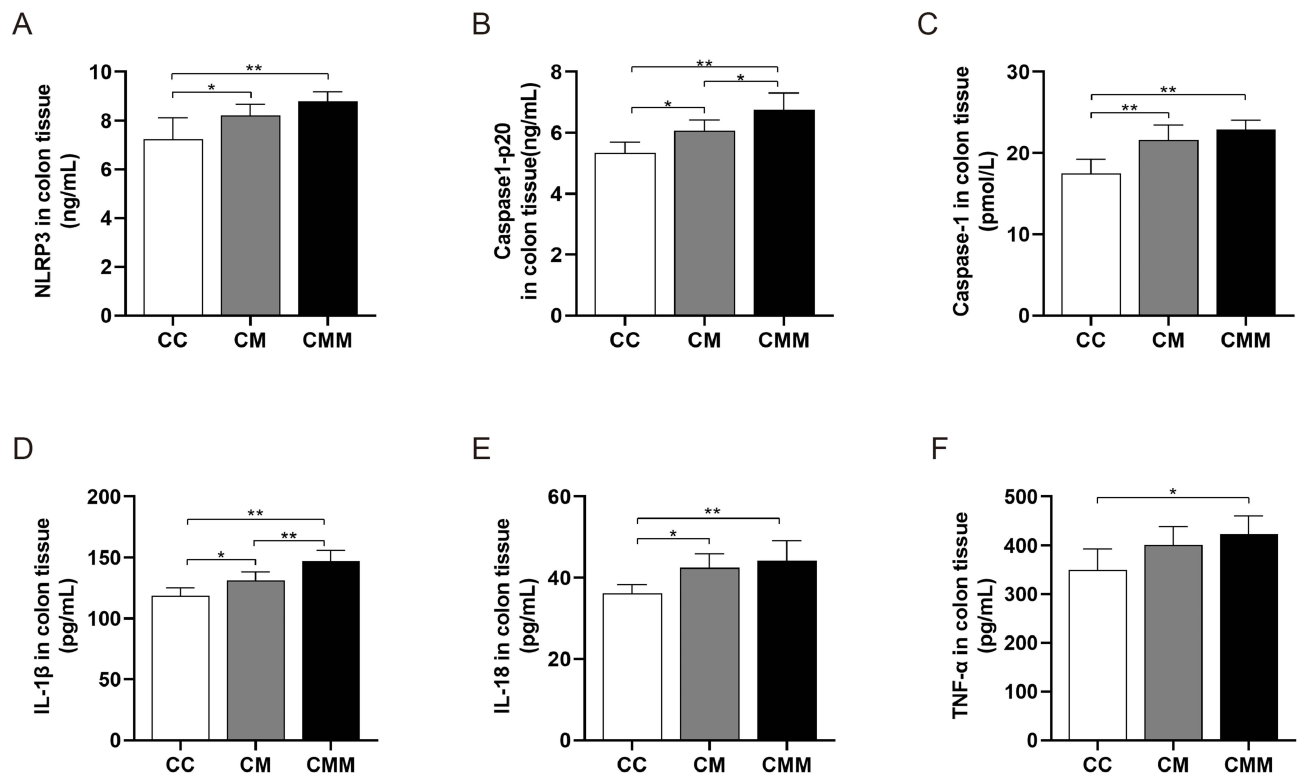


Figure 5 Changes in the levels of NLRP3 inflammasome-related molecules and inflammatory factors in the colonic tissues of mice from various groups. (A) NLRP3 levels in colonic tissue; (B) Caspase-1-p20 levels in colonic tissue; (C) Caspase-1 levels in colonic tissue; (D) IL-1β levels in colonic tissue; (E) IL-18 levels in colonic tissue; (F) TNF-α levels in colonic tissue (n=6). * $p < 0.05$; ** $p < 0.01$.

Abbreviations: CC, control group; CM, diarrhea with kidney-yang deficiency syndrome group; CMM, intestinal microbiota dysbiosis + diarrhea with kidney-yang deficiency syndrome group.

p20, IL-1β, IL-18, and TNF-α were observed in kidney tissues of mice with diarrhea with kidney-yang deficiency syndrome (Figure 6).

Changes in Alpha and Beta Diversity of Intestinal Microbiota

Alpha diversity is a crucial indicator for assessing species richness, diversity, and evenness within a specific community. The rarefaction curve is a crucial indicator for assessing sequencing depth, indirectly reflecting the species richness in the

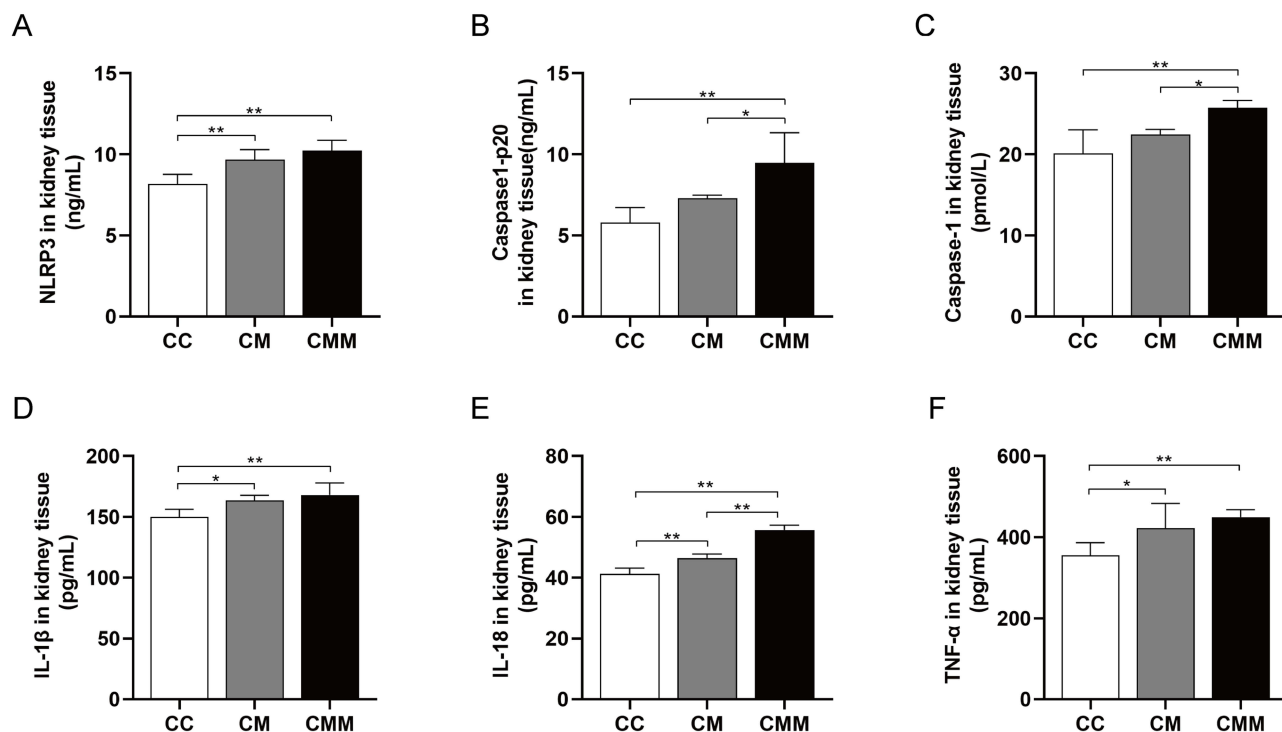


Figure 6 Changes in the levels of NLRP3 inflammasome-related molecules and inflammatory factors in the kidney tissues of mice from various groups. (A) NLRP3 levels in kidney tissue; (B) Caspase-1-p20 levels in kidney tissue; (C) Caspase-1 levels in kidney tissue; (D) IL-1 β levels in kidney tissue; (E) IL-18 levels in kidney tissue; (F) TNF- α levels in kidney tissue (n=6). * $p < 0.05$; ** $p < 0.01$.

Abbreviations: CC, control group; CM, diarrhea with kidney-yang deficiency syndrome group; CMM, intestinal microbiota dysbiosis + diarrhea with kidney-yang deficiency syndrome group.

sample. As shown in Figures 7A and B, both the Shannon rarefaction curve and the Chao1 rarefaction curve gradually become flatter with an increase in the sequencing depth of the samples. The flattening of the curves suggests that no additional ASVs would be detected and that the sequencing depth is sufficient. The Chao1 index reflects species richness. As shown in Figure 7C, compared with the CC and CM groups, the Chao1 index in the CMM group is significantly decreased ($p < 0.01$). Pielou's evenness index represents species evenness. As illustrated in Figure 7D, compared with the CC group, the Pielou's evenness index in the CM group is lower, but the difference is not statistically significant ($p > 0.05$), whereas the Pielou's evenness index in the CMM group is significantly decreased ($p < 0.05$). The Shannon and Simpson indices reflect species diversity. As shown in Figures 7E and F, compared with the CC group, the Shannon index is significantly decreased in both the CM and CMM groups ($p < 0.01$). The Simpson index is lower in the CM group, but the difference is not statistically significant ($p > 0.05$), whereas the Simpson index in the CMM group is significantly decreased ($p < 0.01$).

Beta diversity is an important indicator reflecting the differences in species composition among communities. In the PCoA analysis (Figure 7G), the contribution rates of the horizontal axis (PCo1) and vertical axis (PCo2) are 36.7% and 11.8%, respectively. The CC and CM group samples are projected relatively close without overlapping, while the CMM group exhibits significant dispersion. In the NMDS analysis (Figure 7H), the stress value is 0.058. When this value is less than 0.2, it indicates that the results of the NMDS analysis are reasonable. These findings suggest significant changes in the intestinal microbiota structure of colonic contents in mice with diarrhea with kidney-yang deficiency syndrome.

Changes in Species Composition of Intestinal Microbiota

Under the influence of different interventional factors, variations were observed in the number of taxonomic levels within the intestinal microbial communities (Figure 8A). Figure 8B displays the top 10 most abundant phyla in the colonic microbiota. The top three phyla in abundance in the CC group were Firmicutes (53.76%), Bacteroidota (32.16%), and

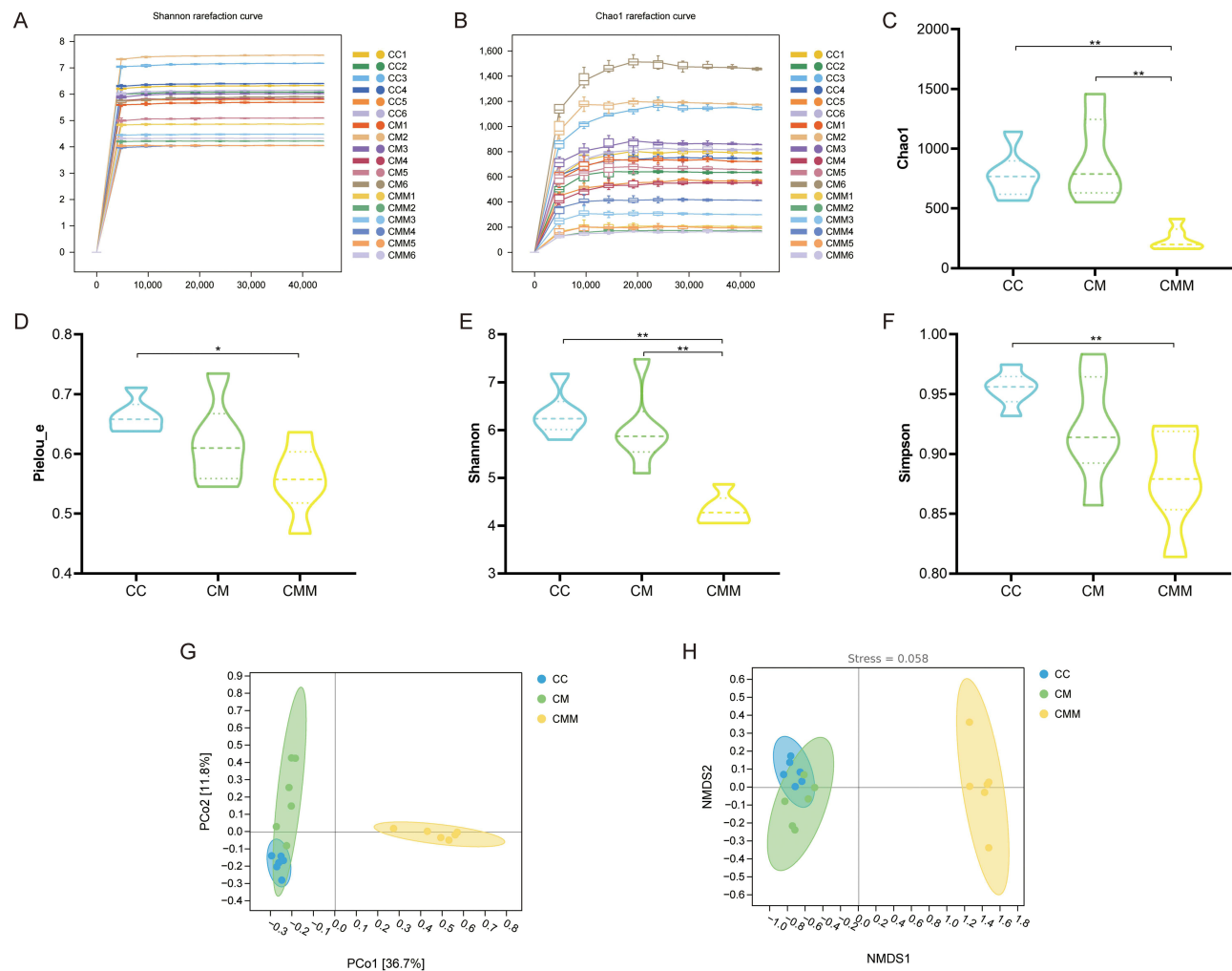


Figure 7 Analysis of intestinal microbiota Alpha and Beta diversity. **(A)** Shannon rarefaction curve; **(B)** Chao1 rarefaction curve; **(C)** Chao1 index; **(D)** Pielou's evenness index; **(E)** Shannon index; **(F)** Simpson index; **(G)** PCoA analysis; **(H)** NMDS analysis. * $p < 0.05$; ** $p < 0.01$.

Abbreviations: CC, control group; CM, diarrhea with kidney-yang deficiency syndrome group; CMM, intestinal microbiota dysbiosis + diarrhea with kidney-yang deficiency syndrome group.

Spirochaetota (3.73%). In the CM group, the top three phyla in abundance were Firmicutes (62.19%), Bacteroidota (30.24%), and Desulfobacterota (2.54%). For the CMM group, the top three phyla in abundance were Bacteroidota (49.22%), Firmicutes (30.57%), and Proteobacteria (14.43%). **Figure 8C** presents the top 15 most abundant genera in the intestinal microbiota. The top five genera in abundance in the CC group were *Lactobacillus* (13.06%), *Alistipes_A* (10.16%), *Ligilactobacillus* (7.46%), *Odoribacter* (6.2%), and *Limosilactobacillus* (6.18%). In the CM group, the top five genera in abundance were *Kurthia* (14.07%), *Ligilactobacillus* (12.2%), *Lactobacillus* (9.73%), *Alloprevotella* (5.01%), and *Duncaniella* (4.92%). For the CMM group, the top five genera in abundance were *Bacteroides_H* (37.6%), *Parabacteroides_B* (7.9%), *Klebsiella* (7.39%), *Blautia_A* (6.59%), and *Coprobacillus* (6.58%).

Subsequently, statistical analysis was performed on the relative abundances of Firmicutes, Bacteroidota, *Bacteroides_H*, *Lactobacillus*, and *Ligilactobacillus* across the groups (**Figure 8D–I**). The relative abundance of Firmicutes in the CMM group was significantly lower than that in the CC and CM groups ($p < 0.01$). The relative abundance of Bacteroidota in the CMM group was significantly higher than that in the CC and CM groups ($p < 0.01$). Compared with either the CC or CM group, the Firmicutes/Bacteroidota ratio in the CMM group was significantly decreased ($p < 0.05$ and $p < 0.01$, respectively). The relative abundance of *Bacteroides_H* in the CMM group was significantly higher than that in the CC and CM groups ($p < 0.01$). Compared with the CC group, the relative abundance of *Lactobacillus* was decreased in both the CM and CMM groups, while

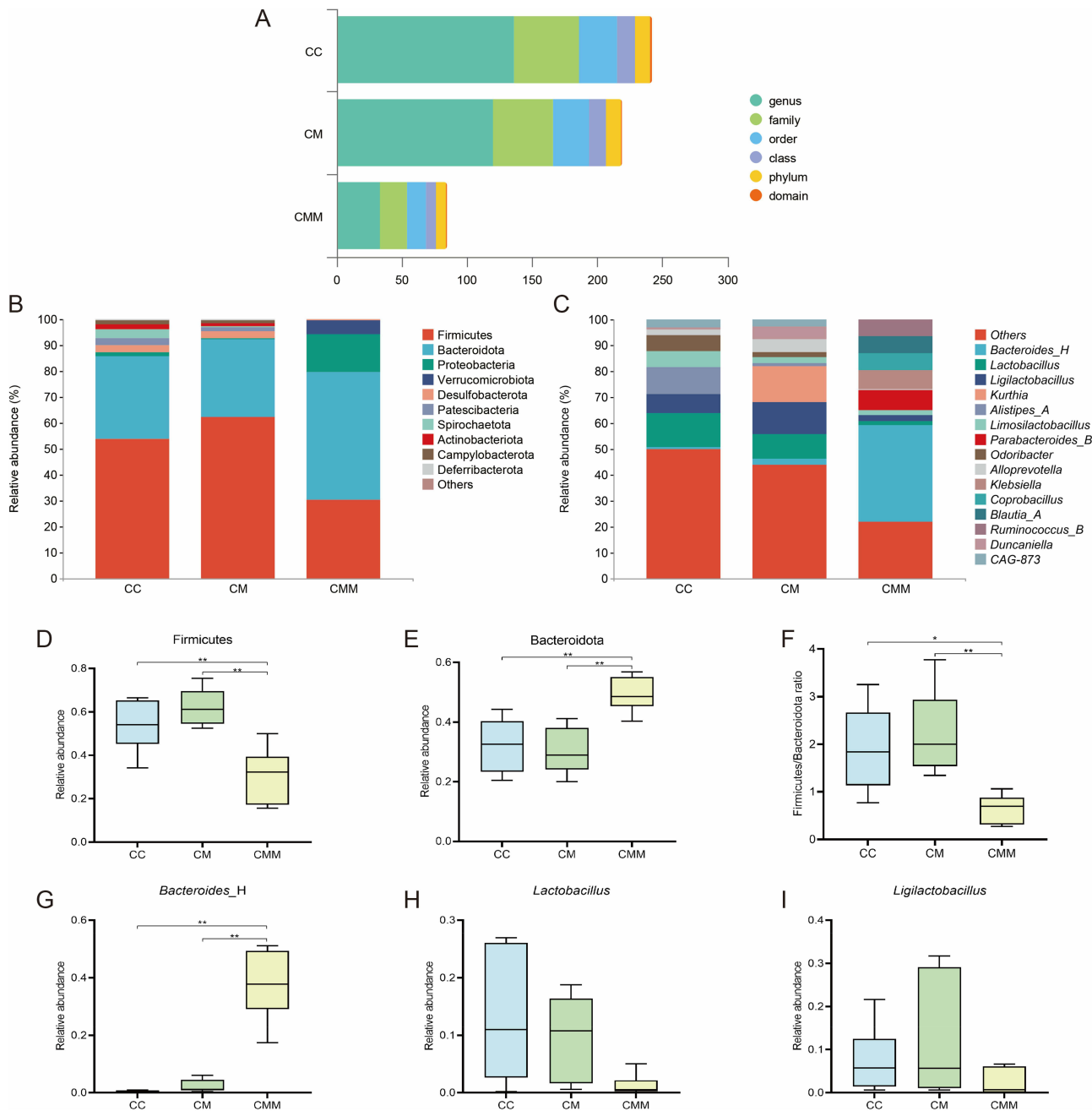


Figure 8 Analysis of intestinal microbiota species composition. (A) Number of taxonomic units at various classification levels; (B) Relative abundance of the top ten most abundant phylum; (C) Relative abundance of the top fifteen most abundant genus; (D) Statistical chart of Firmicutes relative abundance; (E) Statistical chart of Bacteroidota relative abundance; (F) Statistical chart of Firmicutes/Bacteroidota ratio; (G) Statistical chart of *Bacteroides_H* relative abundance; (H) Statistical chart of *Lactobacillus* relative abundance; (I) Statistical chart of *Ligilactobacillus* relative abundance. * $p < 0.05$; ** $p < 0.01$.

Abbreviations: CC, control group; CM, diarrhea with kidney-yang deficiency syndrome group; CMM, intestinal microbiota dysbiosis + diarrhea with kidney-yang deficiency syndrome group.

the relative abundance of *Ligilactobacillus* was increased in the CM group and decreased in the CMM group; however, these differences were not statistically significant ($p > 0.05$).

Characteristic Alterations in the Intestinal Microbiota of Colon Contents

As shown in Figure 9A, LEfSe analysis was performed with an LDA threshold set at >2 to identify robust differential species across all taxonomic levels between groups. Actinobacteriota was a significantly different phylum-level species in the CC group.

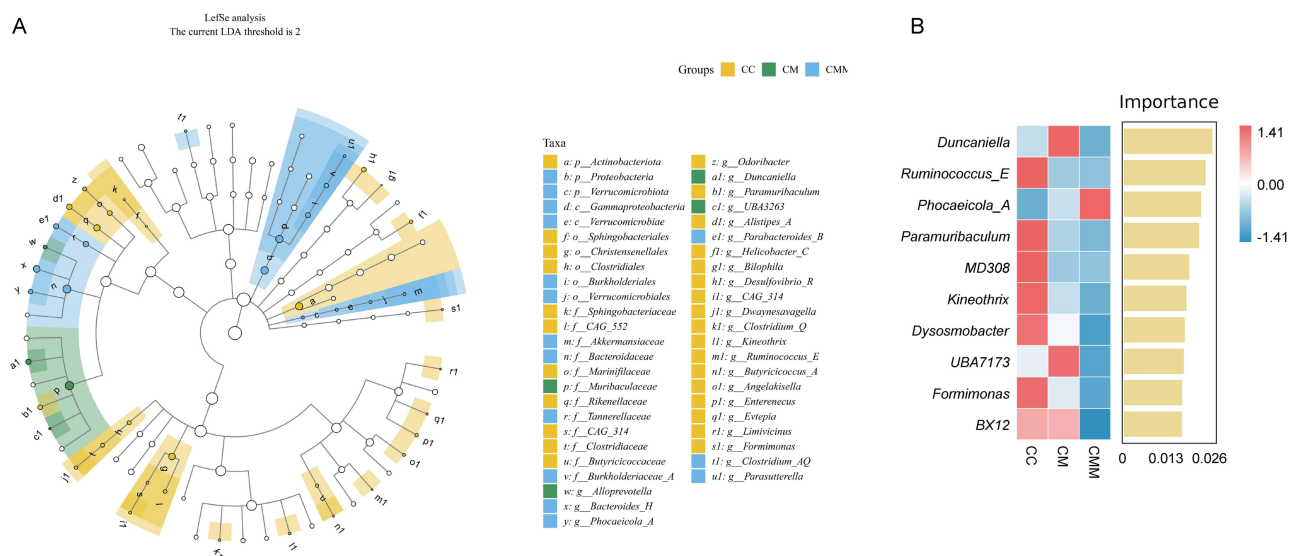


Figure 9 Analysis of characteristic microbiota in colonic contents. **(A)** Cladogram from LEfSe analysis. **(B)** Importance ranking plot of the top 10 species selected by random forest analysis.

Abbreviations: CC, control group; CM, diarrhea with kidney-yang deficiency syndrome group; CMM, intestinal microbiota dysbiosis + diarrhea with kidney-yang deficiency syndrome group.

Proteobacteria and Verrucomicrobiota were significantly different phylum-level species in the CMM group. There were 17 significantly different genus-level species in the CC group, including *Odoribacter*, *Paramuribaculum*, *Alistipes_A*, *Helicobacter_C*, *Bilophila*, among others. *Alloprevotella*, *Duncaniella*, and *UBA3263* were significantly different genus-level species in the CM group. *Bacteroides_H*, *Phocaeicola_A*, *Parabacteroides_B*, *Clostridium_AQ*, and *Parasutterella* were significantly different genus-level species in the CMM group. To further identify the signature species among the three groups of samples, we employed Random Forest analysis to select the top 10 bacterial genera ranked by importance (Figure 9B). In descending order of importance, they are: *Duncaniella*, *Ruminococcus_E*, *Phocaeicola_A*, *Paramuribaculum*, *MD308*, *Kineothrix*, *Dysosmobacter*, *UBA7173*, *Formimonas*, and *BX12*. Therefore, we will proceed to conduct correlation analysis using these 10 important bacterial genera selected by Random Forest analysis.

Correlation Analysis of NLRP3, IL-1 β , IL-18 in Colon and Kidney Tissues with Characteristic Microbiota

To explore the pathological mechanisms of intestinal microbiota dysbiosis and gut-kidney interaction in the progression of diarrhea with kidney-yang deficiency syndrome, we selected the top 10 most important characteristic microbiota based on the random forest analysis. Spearman correlation analysis was performed between NLRP3, IL-1 β , and IL-18 in colonic and kidney tissues and the characteristic microbiota (Figure 10A and B). The levels of NLRP3, IL-1 β , and IL-18 in colonic and kidney tissues were significantly positively correlated with *Phocaeicola_A*. In the colon, there were significant negative correlations between the levels of NLRP3, IL-1 β , and IL-18 and the intestinal microbiota *Ruminococcus_E*, *Kineothrix*, *MD308*, *Paramuribaculum*, and *BX12*. Additionally, the levels of IL-1 β and IL-18 in the colon exhibited significant negative correlations with *Formimonas* and *Dysosmobacter*. Furthermore, a significant negative correlation was observed between the levels of NLRP3 and IL-1 β in the colon and *UBA7173*. In the kidney, the levels of NLRP3, IL-1 β , and IL-18 were significantly negatively correlated with the intestinal microbiota *Dysosmobacter*, *Formimonas*, *Ruminococcus_E*, *Paramuribaculum*, *Kineothrix*, and *MD308*. Moreover, the levels of NLRP3 and IL-18 in the kidney showed significant negative correlations with *BX12*, and the level of IL-18 in the kidney was significantly negatively correlated with *UBA7173*. As shown in Figure 10C and D, red arrows in the RDA analysis represent cytokines, while blue arrows represent characteristic microbiota. When the red and blue arrows form an acute angle, it indicates a positive correlation between them. Conversely, when they form an obtuse angle, it suggests a negative correlation. The levels of NLRP3, IL-1 β , and IL-18 in colonic and renal tissues

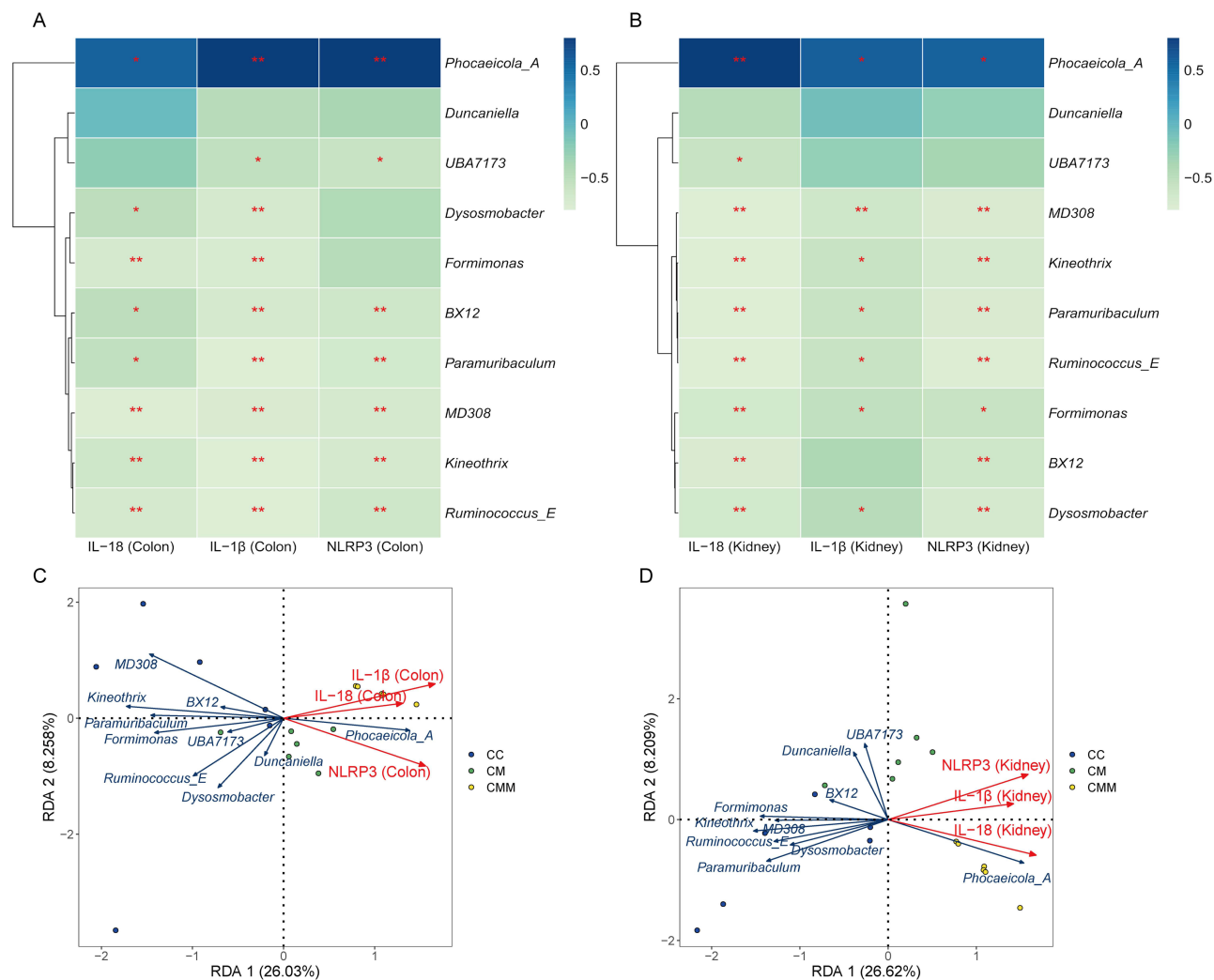


Figure 10 Correlation analysis between NLRP3, IL-1β, IL-18 in colonic and kidney tissues and characteristic microbiota. **(A)** Heatmap showing correlation between NLRP3, IL-1β, IL-18 in the colon and characteristic microbiota; **(B)** Heatmap showing correlation between NLRP3, IL-1β, IL-18 in the kidney tissue and characteristic microbiota; **(C)** RDA analysis of the relationship between NLRP3, IL-1β, IL-18 in the colon and characteristic microbiota; **(D)** RDA analysis of the relationship between NLRP3, IL-1β, IL-18 in the kidney tissue and characteristic microbiota. * $p < 0.05$; ** $p < 0.01$. **Abbreviations:** CC, control group; CM, diarrhea with kidney-yang deficiency syndrome group; CMM, intestinal microbiota dysbiosis + diarrhea with kidney-yang deficiency syndrome group.

were positively correlated with the relative abundance of *Phocaeicola_A* and negatively correlated with other characteristic microbiota. This result is consistent with the findings from the Spearman correlation analysis.

Alterations in Intestinal Microbiota Metabolic Pathways

Our findings revealed that the intestinal microbiota in this study primarily encompassed seven primary metabolic pathways: Biosynthesis, Degradation/Utilization/Assimilation, Detoxification, Generation of Precursor Metabolite and Energy, Glycan Pathways, Macromolecule Modification, and Metabolic Clusters. These primary pathways encompassed a total of 59 secondary metabolic pathways, with the Biosynthesis pathway exhibiting the highest abundance (Figure 11A). Subsequently, we presented the secondary and tertiary metabolic pathways within the Biosynthesis category (Figure 11B). The Biosynthesis category encompassed 12 secondary metabolic pathways: Amine and Polyamine Biosynthesis, Amino Acid Biosynthesis, Aminoacyl-tRNA Charging, Aromatic Compound Biosynthesis, Carbohydrate Biosynthesis, Cell Structure Biosynthesis, Cofactor, Prosthetic Group, Electron Carrier, and Vitamin Biosynthesis, Fatty Acid and Lipid Biosynthesis, Metabolic

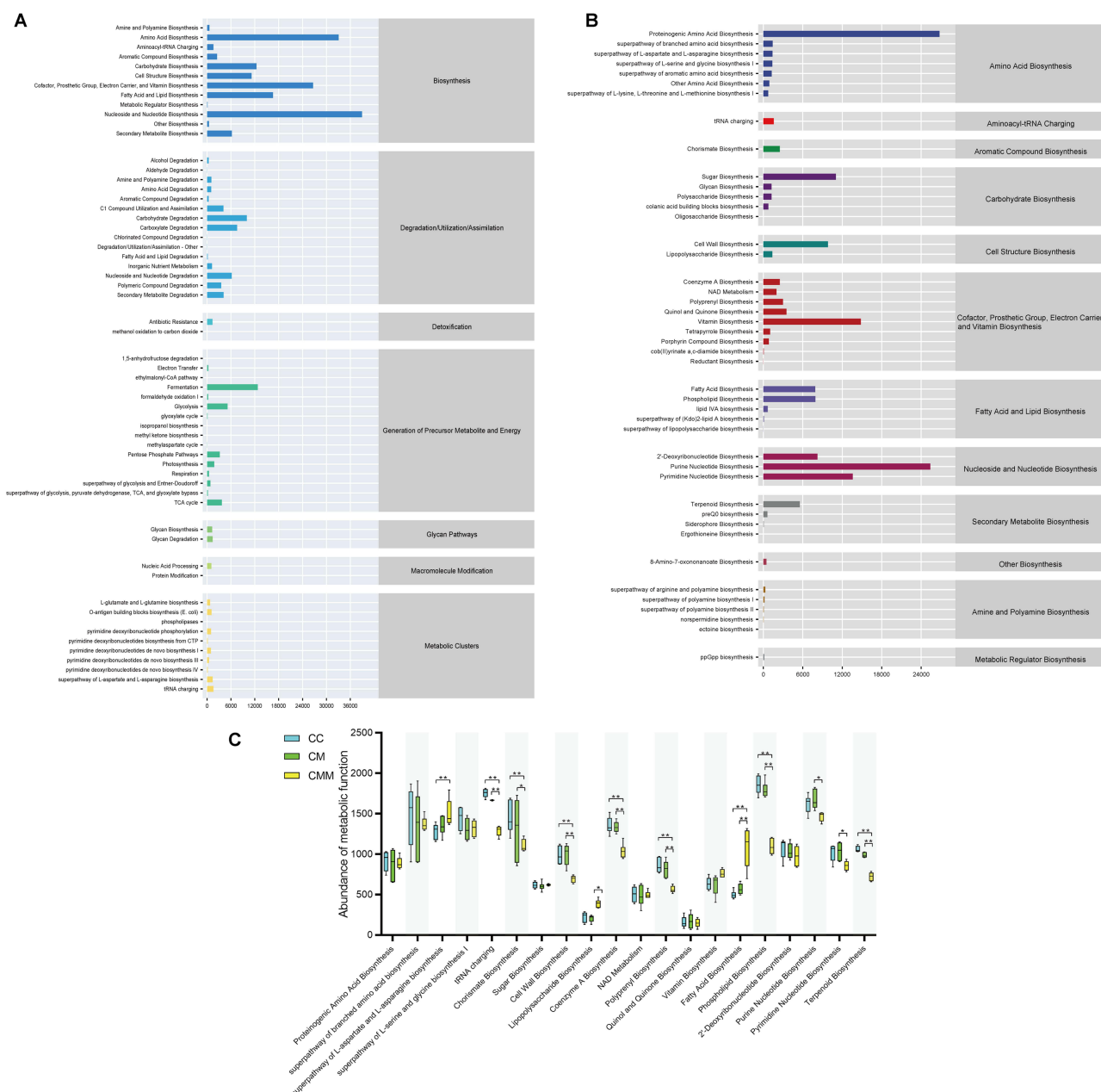


Figure 11 Functional analysis of the intestinal microbiota in mouse colon contents. **(A)** Abundance of MetaCyc secondary metabolic pathways; **(B)** Abundance of MetaCyc tertiary metabolic pathways; **(C)** Statistical analysis of the top 20 tertiary metabolic pathways within the Biosynthesis category. * $p < 0.05$; ** $p < 0.01$.

Abbreviations: CC, control group; CM, diarrhea with kidney-yang deficiency syndrome group; CMM, intestinal microbiota dysbiosis + diarrhea with kidney-yang deficiency syndrome group.

Regulator Biosynthesis, Nucleoside and Nucleotide Biosynthesis, Other Biosynthesis, and Secondary Metabolite Biosynthesis. These secondary pathways encompassed a total of 44 tertiary metabolic pathways.

Among the 44 tertiary metabolic pathways, we selected the top 20 pathways based on their abundance for statistical analysis (Figure 11C). Compared to the CC group, the superpathway of L-aspartate and L-asparagine biosynthesis was significantly upregulated in the CMM group ($p < 0.01$). In comparison to both the CC and CM groups, the CMM group showed significant downregulation in tRNA charging, Cell Wall Biosynthesis, Coenzyme A Biosynthesis, Polypropenyl Biosynthesis, Phospholipid Biosynthesis, and Terpenoid Biosynthesis ($p < 0.01$). Compared to the CC and CM groups, the CMM group exhibited significant downregulation of Chorismate Biosynthesis ($p < 0.01$, $p < 0.05$). In comparison to the CM group, the CMM group showed significant upregulation of Lipopolysaccharide Biosynthesis ($p < 0.05$). Compared to both the CC and CM groups, the CMM

group demonstrated significant upregulation of Fatty Acid Biosynthesis ($p < 0.01$). Additionally, in comparison to the CM group, the CMM group showed significant downregulation of Purine Nucleotide Biosynthesis and Pyrimidine Nucleotide Biosynthesis ($p < 0.01$). Overall, through metabolic pathway prediction, we found that diarrhea with kidney-yang deficiency syndrome may be related to metabolic dysfunction.

Discussion

Pathological Changes in the Colon and Kidney are Key Pathological Characteristics of the Diarrhea with Kidney-Yang Deficiency Syndrome Mouse Model

Diarrhea, characterized by loose or watery stools and an increased frequency of defecation, is a common symptom of various diseases. TCM posits that the intestine is the crucial site of pathology in diarrhea with kidney-yang deficiency syndrome, which is also closely related to the kidney. In this study, mice with kidney-yang deficiency syndrome and diarrhea exhibited poor mental status, loose and unformed feces with increased water content, and decreased body temperature, indicating that the model mice exhibited the typical features of diarrhea with kidney-yang deficiency syndrome.

Through histomorphological observation of colonic tissues in the model mice, we identified structural abnormalities, an increase in the number of inflammatory cells, and the presence of inflammatory infiltration. A properly functioning intestinal barrier constitutes a vital line of defense for maintaining the local microenvironment and overall health of the organism. The intestinal physical barrier is primarily regulated by tight junctions (TJs), with TJ permeability determining the overall barrier function of the intestinal epithelium.²⁸ ZO-1 and occludin are the primary TJ proteins in the intestine. Specifically, ZO-1 serves as a scaffolding protein to maintain the stability of TJ structure, while occludin functions as a transmembrane protein to uphold the normal function of the paracellular pathway.²⁹ When the intestinal barrier is compromised, the intestinal epithelium releases DAO into the bloodstream, making serum DAO levels one of the indicators for assessing intestinal permeability.³⁰ We observed decreased levels of occludin and ZO-1, alongside increased levels of serum DAO, in the colonic tissues of mice presenting with diarrhea with kidney-yang deficiency syndrome. Model mice exhibited pathological alterations in the renal cortex, including structural abnormalities, an increase in inflammatory cells, and dilation and congestion of interstitial blood vessels. Additionally, serum levels of BUN and Cr were significantly elevated, indicating renal structural damage and impaired renal function in mice with diarrhea with kidney-yang deficiency syndrome. Notably, the pathological changes observed in both the colon and kidney represent significant pathological features in the model mice with diarrhea with kidney-yang deficiency syndrome. Loss of intestinal barrier integrity is one of the pathways by which microorganisms and their derived molecules affect distant organs, resulting in pathogenic interactions along the gut-target organ axis (eg, liver, lung).³¹ Therefore, in the progression of diarrhea with kidney-yang deficiency syndrome, impairment of intestinal barrier function may be a crucial factor contributing to the exacerbation of the disease.

NLRP3 Inflammasome-Related Molecules and Inflammatory Factors Participate in the Gut-Kidney Interaction Damage in a Mouse Model of Diarrhea with Kidney-Yang Deficiency Syndrome

The NLRP3 inflammasome is a multiprotein complex primarily located in the cytoplasm of myeloid lineage cells (eg, macrophages, dendritic cells, and neutrophils), which are key players in innate immunity. It consists of three key components: the innate immune receptor protein NLRP3, the adapter protein ASC, and the inflammatory protease caspase-1.³² It responds to microbial infections, endogenous danger signals, and external stimuli. Caspase-1 is primarily activated by the NLRP3 inflammasome, which converts pro-caspase-1 into active caspase-1-p20. Caspase-1-p20 then leads to the maturation of pro-inflammatory cytokines IL-1 β and IL-18, initiating various downstream signaling pathways and triggering the inflammatory response in the body.^{33,34} Studies have shown that the NLRP3/Caspase-1 signaling pathway, along with inflammatory cytokines such as IL-1 β and TNF- α , is involved in the pathogenesis of diarrhea, leading to intestinal oxidative damage and inflammatory responses.³⁵ In our team's previous research, it was found that intestinal microbiota metabolites can activate

inflammatory responses and cytokines, resulting in a significant increase in NLRP3 and IL-1 β levels in the serum of model mice, thereby affecting diarrhea with kidney-yang deficiency syndrome through the “gut-kidney axis”.³⁶

In this experiment, we conducted a further investigation into the mouse model of diarrhea with kidney-yang deficiency syndrome. By measuring the levels of NLRP3, Caspase-1, Caspase1-p20, IL-1 β , IL-18, and TNF- α in colonic and kidney tissues, we found that these parameters exhibited varying degrees of increase across both tissues, with the CMM group showing higher levels of NLRP3 inflammasome-related molecules and inflammatory factors compared to the CM group. This finding indicates that NLRP3 inflammasome-related molecules and inflammatory factors are not only involved in the inflammatory response within colonic tissue but may also exert an influence on kidney tissue through some mechanism, thereby facilitating the gut-kidney interaction. Therefore, we infer that NLRP3 inflammasome-related molecules and inflammatory factors are involved in the gut-kidney interaction in the mouse model of diarrhea with kidney-yang deficiency syndrome, and are crucial contributors to the tissue damage and inflammatory infiltration observed in both colonic and kidney tissues.

Dysbiosis of Intestinal Microbiota Is a Key Link in the Gut-Kidney Interaction in a Mouse Model of Diarrhea with Kidney-Yang Deficiency Syndrome

The intestinal microbiota maintains a mutualistic relationship with the host and plays essential roles in nutrient metabolism (eg, primary bile acids, vitamins, etc.), immune regulation, and maintaining the integrity of the intestinal barrier and gastrointestinal structure in healthy individuals.³⁷ Under the influence of various risk factors, the phenotype of commensal bacteria may shift from beneficial to pathogenic, and disruptions in the structure and metabolic function of the intestinal microbiota are key factors contributing to the onset and/or progression of various gastrointestinal diseases.³⁸ Previous studies have demonstrated that mice with diarrhea with kidney-yang deficiency syndrome exhibit intestinal microbiota dysbiosis, and this dysbiosis may exert detrimental effects on the diarrhea with kidney-yang deficiency syndrome by altering the levels of inflammatory cytokines such as TNF- α and IL-6.³⁹ In this study, we designed three groups: a control group, a group with diarrhea with kidney-yang deficiency syndrome, and a group with intestinal microbiota dysbiosis + diarrhea with kidney-yang deficiency syndrome. By establishing a mouse model with compound factors, we further elucidated the specific mechanisms involved in the participation of intestinal dysbiosis in diarrhea with kidney-yang deficiency syndrome.

In this study, compared to the CC group, alterations in the microbial diversity of colonic contents were observed in both the CM and CMM groups. The Chao1 index was significantly decreased in the CMM group ($p < 0.01$). There was a decreasing trend in Pielou's evenness, Shannon index, and Simpson index in the CM group, and these indices were even lower in the CMM group. The alpha diversity index generally decreased in the model mice, with a marked reduction in the CMM group. The alpha diversity index is an important indicator for evaluating intestinal microbiota dysbiosis, which represents a state differing from normal or healthy conditions.⁴⁰ In mice with the diarrhea with kidney-yang deficiency syndrome model, the degree of intestinal microbiota dysbiosis became even more pronounced after they were simultaneously fed a mixed antibiotic solution. This also facilitated our observation of the gut-kidney interactions in the model mice under intestinal microbiota dysbiosis. Beta diversity analysis also revealed changes in the intestinal microbiota structure of mice in the CM and CMM groups compared to the CC group. These findings suggest that the mouse model of diarrhea with kidney-yang deficiency syndrome exhibits intestinal microbiota dysbiosis, characterized by decreased microbial richness, diversity, and evenness in colonic contents, as well as a distinct intestinal microbiota structure compared to that of normal mice.

Species composition analysis revealed a significant reduction in the Firmicutes/Bacteroidota ratio in the CMM group. The imbalance in the Firmicutes/Bacteroidota ratio is also recognized as an indicator of dysbiosis in the intestinal microbiota, with similar alterations observed in other inflammatory conditions (including hematological malignancies, type 2 diabetes, and inflammatory bowel disease).⁴¹ Notably, the species composition of the intestinal microbiota in the CMM group exhibited a significant increase in the relative abundance of *Bacteroides_H* following mixed antibiotic treatment. However, its biological significance remains poorly understood. Both *Lactobacillus* and *Ligilactobacillus* exhibited reduced relative abundances in the CMM group. Both genera belong to the family Lactobacillaceae, whose

strains are widely utilized in probiotic development due to their health-promoting effects. Key characteristics of these strains include adhesion and aggregation capabilities, competitive exclusion, autoaggregation/coaggregation behavior, and immunomodulatory functions. For instance, certain strains (eg, *L. rhamnosus* and *L. acidophilus*) have demonstrated efficacy in reducing pathogen adhesion and colonization in competitive adhesion assays,⁴² thereby contributing to the prevention and clearance of gastrointestinal pathogens. In this study, we observed that in diarrhea with kidney-yang deficiency syndrome model mice, concurrent administration of a mixed antibiotic solution induced alterations in intestinal microbiota diversity and species composition, resulting in a more pronounced state of intestinal microbiota dysbiosis. This will facilitate our observation of gut-kidney interactions in model mice under conditions of intestinal microbiota dysbiosis.

Utilizing LefSe analysis and Random Forest analysis, we further identified the top 10 most significant bacterial genera based on their importance rankings. Having identified the top 10 most significant bacterial genera in the previous analysis, subsequently, we conducted correlation analyses between these 10 bacterial genera and the levels of NLRP3, IL-1 β , and IL-18 in colonic and kidney tissues. Our findings revealed a significant positive correlation between the levels of NLRP3, IL-1 β , and IL-18 in both colonic and kidney tissues and the abundance of *Phocaeicola_A*. *Phocaeicola_A* belongs to the bacterial genus within the Bacteroidaceae family. Currently, there is a paucity of research data on *Phocaeicola_A*. Studies have indicated that *Phocaeicola* is significantly more abundant in samples from persistently infected sites.⁴³ Additionally, a higher relative abundance of *Phocaeicola* has been observed in metabolic dysfunction-associated fatty liver induced by high-fat and high-fructose diets.⁴⁴ Furthermore, there are multiple bacterial genera that exhibit significant negative correlations with the levels of NLRP3, IL-1 β , and IL-18 in colonic and kidney tissues. Taking *Paramuribaculum* as an example, this bacterial genus may play a crucial role in the body's anti-inflammatory and immunomodulatory processes.⁴⁵ Additionally, *Paramuribaculum* has the capability to produce propionic and butyric acids, potentially contributing to an increase in fecal short-chain fatty acids (SCFAs) levels.⁴⁶ In particular, butyric acid has been extensively demonstrated to reduce the release of pro-inflammatory cytokines, promote the differentiation of anti-inflammatory regulatory T cells, and mitigate intestinal barrier leakage, thereby participating in the regulation of inflammatory responses and alleviation of colon-related diseases.⁴⁷

Metabolic activities of the intestinal microbiota constitute one of the essential pathways for exerting their biological functions. In this study, metabolic function predictions concentrated on the Biosynthesis section, encompassing 44 tertiary metabolic pathways. Compared to the CC group, significant differences were observed in 12 metabolic pathways, such as Polyphenyl Biosynthesis and Terpenoid Biosynthesis, in the model mice. These results indicate that intestinal microbiota dysbiosis plays a pivotal role in the gut-kidney interaction damage within the mouse model of diarrhea with kidney-yang deficiency syndrome. Intestinal microbiota dysbiosis can disrupt the mucosal barrier, leading to pathological damage in the tissue structures of the colon and kidneys, along with elevated levels of NLRP3 inflammasome-related molecules and inflammatory cytokines. This results in gut-kidney interaction damage, thereby exacerbating diarrhea.

Conclusion

In conclusion, diarrhea with kidney-yang deficiency syndrome is associated with dysbiosis of the intestinal microbiota in the colon, impaired intestinal barrier morphology and function, and elevated levels of NLRP3 inflammasome-related molecules and inflammatory cytokines in colonic and renal tissues, which collectively contribute to pathological damage in these organs. We observed that under the condition of intestinal microbiota dysbiosis, the mouse model of diarrhea with kidney-yang deficiency syndrome exhibited damage to gut-kidney interactions, which exacerbated the diarrhea. This study provides novel insights into the role of intestinal microbiota dysbiosis in the pathogenesis of diarrheal diseases and lays a crucial foundation for future research and therapeutic strategies targeting diarrhea with kidney-yang deficiency syndrome.

Abbreviations

TCM, traditional Chinese medicine; BUN, blood urea nitrogen; Cr, creatinine; NLRP3, NOD-like receptor family pyrin domain containing protein 3; IL, Interleukin; MDA, malondialdehyde; SOD, superoxide dismutase; ZO-1, zonula occludens-1; TGF, transforming growth factor; TNF, tumor necrosis factor; CKD, chronic kidney disease; LPS, lipopolysaccharide; ELISA, enzyme-linked immunosorbent assay; DAO, diamine oxidase; DAB, 3,3'-Diaminobenzidine; AOD, average optical density; OD, optical density; ASVs, amplicon sequence variants; PCoA,

principal coordinates analysis; NMDS, non-metric multidimensional scaling; LefSe, linear discriminant analysis effect size; TJ, tight junctions; SCFAs, short-chain fatty acids.

Data Sharing Statement

The data underlying this study are available within the manuscript. The colon content microbiota sequencing data has been uploaded to the NCBI database (<https://www.ncbi.nlm.nih.gov/>), NO. PRJNA1139051.

Ethics Approval and Informed Consent

The experiment was approved by the Institutional Animal Care and Use Committee of Hunan University of Chinese Medicine and was conducted in accordance with the Laboratory Animal—Guideline for Ethical Review of Animal Welfare (GB/T 35892-2018). (Ethics Number: HNUCM21-2409-14).

Funding

This work was supported by the Postgraduate Scientific Research Innovation Project of Hunan Province (CX20240730).

Disclosure

The authors report no conflicts of interest in this work.

References

1. Al Fidah MF, Haider T, Roy D, et al. Temporal trends of diarrheal diseases and associated treatment responses among children aged under five: insight from the multiple Indicator Cluster surveys from 2006 to 2019. *Pediatr Neonatol.* **2024**;2:S1875–9572(24)00128–1. doi:10.1016/j.pedneo.2024.03.010
2. GBD 2021 Diarrhoeal Diseases Collaborators. Global, regional, and national age-sex-specific burden of diarrhoeal diseases, their risk factors, and aetiologies, 1990–2021, for 204 countries and territories: a systematic analysis for the global burden of disease study 2021. *Lancet Infect Dis.* **2024**. doi:10.1016/S1473-3099(24)00691-1
3. Cheng SX. Calcium-sensing receptor: a new target for therapy of diarrhea. *World J Gastroenterol.* **2016**;22(9):2711–2724. doi:10.3748/wjg.v22.i9.2711
4. Negussie AB, Dell AC, Davis BA, et al. Colonic fluid and electrolyte transport 2022: an update. *Cells.* **2022**;11(10):1712. doi:10.3390/cells11101712
5. Shahrin L, Sarmin M, Rahman AS, et al. Clinical and laboratory characteristics of acute kidney injury in infants with diarrhea: a cross-sectional study in Bangladesh. *J Int Med Res.* **2020**;48(1):300060519896913. doi:10.1177/0300060519896913
6. Lee JR, Magruder M, Zhang L, et al. Gut microbiota dysbiosis and diarrhea in kidney transplant recipients. *Am J Transplant.* **2019**;19(2):488–500. doi:10.1111/ajt.14974
7. Zhu J, Li X, Deng N, et al. Intestinal mucosal flora of the intestine-kidney remediation process of diarrhea with deficiency kidney-yang syndrome in Sishen Pill treatment: association with interactions between *Lactobacillus johnsonii*, Ca²⁺-Mg²⁺-ATP-ase, and Na⁺-K⁺-ATP-ase. *Heliyon.* **2023**;9(5):e16166. doi:10.1016/j.heliyon.2023.e16166
8. Li X, Zhu J, Wu Y, et al. Correlation between kidney function and intestinal biological characteristics of adenine and folium sennae-induced diarrhea model in mice. *Turk J Gastroenterol.* **2023**;34(1):4–12. doi:10.5152/tjg.2022.211010
9. Zhou M, Li X, Wang X, et al. The dysfunction in intestinal microorganisms and enzyme activity as significant contributors to diarrhea with kidney-yang deficiency syndrome. *Front Microbiol.* **2024**;14:1324938. doi:10.3389/fmicb.2023.1324938
10. Xie S, Fang L, Deng N, et al. Targeting the gut-kidney axis in diarrhea with kidney-yang deficiency syndrome: the role of sishen pills in regulating TMAO-mediated inflammatory response. *Med Sci Monit.* **2024**;30:e944185. doi:10.12659/MSM.944185
11. Guo M, Fang L, Chen M, et al. Dysfunction of cecal microbiota and CutC activity in mice mediating diarrhea with kidney-yang deficiency syndrome. *Front Microbiol.* **2024**;15:1354823. doi:10.3389/fmicb.2024.1354823
12. Chen YY, Chen DQ, Chen L, et al. Microbiome-metabolome reveals the contribution of gut-kidney axis on kidney disease. *J Transl Med.* **2019**;17(1):5. doi:10.1186/s12967-018-1756-4
13. Cabala S, Özgo M, Herosimczyk A. The kidney-gut axis as a novel target for nutritional intervention to counteract chronic kidney disease progression. *Metabolites.* **2024**;14(1):78. doi:10.3390/metabo14010078
14. Kurashima Y, Kiyono H. Mucosal ecological network of epithelium and immune cells for gut homeostasis and tissue healing. *Annu Rev Immunol.* **2017**;35:119–147. doi:10.1146/annurev-immunol-051116-052424
15. Sun M, Fang Y, Zheng J, et al. Role of symbiotic microbiota dysbiosis in the progression of chronic kidney disease accompanied with vascular calcification. *Front Pharmacol.* **2024**;14:1306125. doi:10.3389/fphar.2023.1306125
16. Zhu L, Niu J, Tang XC, et al. The effects of probiotic *Lactobacillus rhamnosus* GG on fecal flora and serum markers of renal injury in mice with chronic kidney disease. *Front Biosci.* **2023**;28(9):226. doi:10.31083/j.fbl2809226
17. Wu Y, Peng X, Li X, et al. Sex hormones influence the intestinal microbiota composition in mice. *Front Microbiol.* **2022**;13:964847. doi:10.3389/fmicb.2022.964847
18. Fang L, Shen J, Wu Y, et al. Involvement of intestinal mucosal microbiota in adenine-induced liver function injury. *3 Biotech.* **2025**;15(1):6. doi:10.1007/s13205-024-04180-7

19. Zhu J, Li X, Deng N, et al. Diarrhea with deficiency kidney-yang syndrome caused by adenine combined with Folium senna was associated with gut mucosal microbiota. *Front Microbiol.* **2022**;13:1007609. doi:10.3389/fmicb.2022.1007609
20. Long C, Liu Y, He L, et al. Bacterial lactase genes diversity in intestinal mucosa of mice with dysbacterial diarrhea induced by antibiotics. *3 Biotech.* **2018**;8(3):176. doi:10.1007/s13205-018-1191-5
21. Xie G, Zhou R, Huang L, et al. In vitro biotransformation of total glycosides in qiwei baizhu powder by the gut microbiota of normal and diarrheal mice: novel insight into the biotransformation of multi-glycosides by the gut microbiota. *Front Chem.* **2022**;10:907886. doi:10.3389/fchem.2022.907886
22. Xie G, Tan K, Peng M, et al. Bacterial diversity in intestinal mucosa of antibiotic-associated diarrhea mice. *3 Biotech.* **2019**;9(12):444. doi:10.1007/s13205-019-1967-2
23. Shao H, Zhang C, Xiao N, et al. Gut microbiota characteristics in mice with antibiotic-associated diarrhea. *BMC Microbiol.* **2020**;20(1):313. doi:10.1186/s12866-020-01999-x
24. Yi X, Zhou K, Deng N, et al. Simo decoction curing spleen deficiency constipation was associated with brain-bacteria-gut axis by intestinal mucosal microbiota. *Front Microbiol.* **2023**;14:1090302. doi:10.3389/fmicb.2023.1090302
25. Hui H, Wu Y, Zheng T, et al. Bacterial characteristics in intestinal contents of antibiotic-associated diarrhea mice treated with Qiweibaizhu powder. *Med Sci Monit.* **2020**;26:e921771. doi:10.12659/MSM.921771
26. Shen J, Wu Y, Fang L, et al. Huoxiang Zhengqi decoction ameliorates gastrointestinal disorders induced by cold and humid environmental stress via modulation of intestinal mucosal microbiota and amino acid metabolism. *3 Biotech.* **2025**;15(6):150. doi:10.1007/s13205-025-04324-3
27. Shen J, Fang L, Tan Z, et al. The effects of functional biscuits on intestinal mucosal microbiota composition, brain function, and antioxidant activity. *Biosci Microbiota Food Health.* **2025**;44(2):171–181. doi:10.12938/bmfh.2024-078
28. Turner JR. Molecular basis of epithelial barrier regulation: from basic mechanisms to clinical application. *Am J Pathol.* **2006**;169(6):1901–1909. doi:10.2353/ajpath.2006.060681
29. Zhao X, Zeng H, Lei L, et al. Tight junctions and their regulation by non-coding RNAs. *Int J Biol Sci.* **2021**;17(3):712–727. doi:10.7150/ijbs.45885
30. Chen F, Chen J, Chen Q, et al. Lactobacillus delbrueckii protected intestinal integrity, alleviated intestinal oxidative damage, and activated toll-like receptor-bruton's tyrosine kinase-nuclear factor erythroid 2-related factor 2 pathway in weaned piglets challenged with lipopolysaccharide. *Antioxidants.* **2021**;10(3):468. doi:10.3390/antiox10030468
31. Anand S, Mande SS. Host-microbiome interactions: gut-Liver axis and its connection with other organs. *NPJ Biofilms Microbiomes.* **2022**;8(1):89. doi:10.1038/s41522-022-00352-6
32. Huang Y, Xu W, Zhou R. NLRP3 inflammasome activation and cell death. *Cell Mol Immunol.* **2021**;18(9):2114–2127. doi:10.1038/s41423-021-00740-6
33. Modi P, Shah BM, Patel S. Interleukin-1 β converting enzyme (ICE): a comprehensive review on discovery and development of caspase-1 inhibitors. *Eur J Med Chem.* **2023**;261:115861. doi:10.1016/j.ejmech.2023.115861
34. Li H, Guo Z, Chen J, et al. Computational research of Belnacasan and new Caspase-1 inhibitor on cerebral ischemia reperfusion injury. *Aging.* **2022**;14(4):1848–1864. doi:10.18632/aging.203907
35. Chen X, Kong Q, Zhao X, et al. Sodium acetate/sodium butyrate alleviates lipopolysaccharide-induced diarrhea in mice via regulating the gut microbiota, inflammatory cytokines, antioxidant levels, and NLRP3/Caspase-1 signaling. *Front Microbiol.* **2022**;13:1036042. doi:10.3389/fmicb.2022.1036042
36. Xie S, Deng N, Fang L, et al. TMAO is involved in kidney-yang deficiency syndrome diarrhea by mediating the “gut-kidney axis”. *Heliyon.* **2024**;10(15):e35461. doi:10.1016/j.heliyon.2024.e35461
37. Jandhyala SM, Talukdar R, Subramanyam C, et al. Role of the normal gut microbiota. *World J Gastroenterol.* **2015**;21(29):8787–8803. doi:10.3748/wjg.v21.i29.8787
38. Nagao-Kitamoto H, Kitamoto S, Kuffa P, et al. Pathogenic role of the gut microbiota in gastrointestinal diseases. *Intest Res.* **2016**;14(2):127–138. doi:10.5217/ir.2016.14.2.127
39. Guo M, Wu Y, Peng M, et al. Decreasing of Trimethylamine N-Oxide by cecal microbiota and choline-trimethylamine lyase are associated with sishen pill on diarrhea with kidney-yang deficiency syndrome. *J Inflamm Res.* **2024**;17:7275–7294. doi:10.2147/JIR.S470254
40. Wei S, Bahl MI, Baunwall SMD, et al. Determining gut microbial dysbiosis: a review of applied indexes for assessment of intestinal microbiota imbalances. *Appl Environ Microbiol.* **2021**;87(11):e00395–21. doi:10.1128/AEM.00395-21
41. Paziewska M, Kielbus M, Szelest M, et al. Increased abundance of Firmicutes and depletion of Bacteroidota predicts poor outcome in chronic lymphocytic leukemia. *Oncol Lett.* **2024**;28(5):552. doi:10.3892/ol.2024.14685
42. Santos AA, Duarte R, Duarte M, et al. Impact of Lactobacillaceae supplementation on the multi-organ axis during MASLD. *Life Sci.* **2024**;354:122948. doi:10.1016/j.lfs.2024.122948
43. Sun X, Yang Z, Nie Y, et al. Microbial communities in the extraradicular and intraradicular infections associated with persistent apical periodontitis. *Front Cell Infect Microbiol.* **2022**;11:798367. doi:10.3389/fcimb.2021.798367
44. Choi KJ, Yoon MY, Kim JE, et al. Gut commensal Kineothrix alysoidea mitigates liver dysfunction by restoring lipid metabolism and gut microbial balance. *Sci Rep.* **2023**;13(1):14668. doi:10.1038/s41598-023-41160-y
45. Liu S, Wang B, Chen T, et al. Two new and effective food-extracted immunomodulatory agents exhibit anti-inflammatory response activity in the hACE2 acute lung injury murine model of COVID-19. *Front Immunol.* **2024**;15:1374541. doi:10.3389/fimmu.2024.1374541
46. Watanabe K, Yamano M, Masujima Y, et al. Curd intake changes gut microbial composition, short-chain fatty acid production, and bile acid transformation in mice. *Biochem Biophys Res.* **2021**;27:101095. doi:10.1016/j.bbrep.2021.101095
47. Hays KE, Pfaffinger JM, Ryznar R. The interplay between gut microbiota, short-chain fatty acids, and implications for host health and disease. *Gut Microbes.* **2024**;16(1):2393270. doi:10.1080/19490976.2024.2393270

Journal of Inflammation Research

Dovepress
Taylor & Francis Group

Publish your work in this journal

The Journal of Inflammation Research is an international, peer-reviewed open-access journal that welcomes laboratory and clinical findings on the molecular basis, cell biology and pharmacology of inflammation including original research, reviews, symposium reports, hypothesis formation and commentaries on: acute/chronic inflammation; mediators of inflammation; cellular processes; molecular mechanisms; pharmacology and novel anti-inflammatory drugs; clinical conditions involving inflammation. The manuscript management system is completely online and includes a very quick and fair peer-review system. Visit <http://www.dovepress.com/testimonials.php> to read real quotes from published authors.

Submit your manuscript here: <https://www.dovepress.com/journal-of-inflammation-research-journal>